Structure
Article

The Structural Basis for the Function of Two Anti-VEGF Receptor 2 Antibodies

Matthew C. Franklin,[1,5,*] Elizabeth C. Navarro,[2] Yujie Wang,[3] Sheetal Patel,[4] Pinki Singh,[4] Yi Zhang,[1] Kris Persaud,[4] Amtul Bari,[4] Heather Griffith,[2] Leyi Shen,[2] Paul Balderes,[2] and Paul Kussie[3]
[1]Department of Immunology
[2]Department of Bioprocess Science
[3]Department of Protein Science
[4]Department of Molecular and Cellular Engineering
ImClone Systems, New York, NY 10014, USA
[5]Present address: New York Structural Biology Center, 89 Convent Avenue, New York, NY 10027, USA
*Correspondence: mfranklin@nysbc.org
DOI 10.1016/j.str.2011.01.019

SUMMARY

The anti-VEGF receptor 2 antibody IMC-1121B is a promising antiangiogenic drug being tested for treatment of breast and gastric cancer. We have determined the structure of the 1121B Fab fragment in complex with domain 3 of VEGFR2, as well as the structure of a different neutralizing anti-VEGFR2 antibody, 6.64, also in complex with VEGFR2 domain 3. The two Fab fragments bind at opposite ends of VEGFR2 domain 3; 1121B directly blocks VEGF binding, whereas 6.64 may prevent receptor dimerization by perturbing the domain 3:domain 4 interface. Mutagenesis reveals that residues essential for VEGF, 1121B, and 6.64 binding are nonoverlapping among the three contact patches.

INTRODUCTION

The process of blood vessel growth and maturation is fundamentally important to the growth and survival of all animals with a circulatory system (Roskoski, 2007b). New blood vessels can develop from two closely related processes: vasculogenesis, the assembly of vessels from precursor cells, and angiogenesis, the sprouting of new vessels from a preexisting network (Roskoski, 2007b). Both processes are critical during embryonic development, and angiogenesis remains essential in the mature organism, especially for functions such as wound repair and growth of the endometrial lining (Ferrara, 2004; Folkman, 1995). However, angiogenesis also underlies a number of pathological processes, including diabetic retinopathy, age-related macular degeneration, and psoriasis (Chua and Arbiser, 2009; Ferrara, 2004). In particular, angiogenesis is necessary for the pathogenesis of solid tumors, which are unable to grow beyond a small size without the formation of an extensive vascular network (Folkman, 1995).

The key players in the process of angiogenesis are the vascular endothelial growth factors (VEGFs) and their receptors. In humans, there are four closely related VEGF molecules, designated VEGF-A, -B, -C, and -D (Roskoski, 2007b), and three known VEGF receptors: VEGFR1, also known as Flt-1 (fms-like tyrosine kinase 1) (de Vries et al., 1992; Shibuya et al., 1990); VEGFR2, also known as KDR (kinase insert domain receptor) (Terman et al., 1991, 1992); and VEGFR3, or Flt-4 (Pajusola et al., 1992). The VEGF receptors are class V of the receptor tyrosine kinases (Grassot et al., 2006), and contain seven Ig-like domains in their extracellular portion, a single transmembrane helix, and an intracellular kinase domain (Ferrara, 2004; Roskoski, 2008). Of all the possible interactions between these ligands and receptors, the most important for angiogenesis is the one between VEGF-A and KDR (Ferrara, 2004; Shalaby et al., 1995). Flt-1 may represent a regulatory ''decoy'' receptor for VEGF-A and -B (Hiratsuka et al., 1998; Meyer et al., 2006; Park et al., 1994), whereas VEGF-C and -D interactions with Flt-4 are primarily important in lymphangiogenesis (Kaipainen et al., 1995; Tammela and Alitalo, 2010). Mature VEGF-A (hereafter referred to simply as VEGF) is a disulfide-linked homodimer in which the receptor binding domain contains two identical binding sites, at opposite ends of the domain, formed by residues from both chains (Wiesmann et al., 1997). Bound VEGF is therefore thought to bridge two receptor molecules, forming a dimer; this hypothesis is supported by electron microscopy of VEGF:KDR complexes (Ruch et al., 2007). A KDR homodimer is thought to be the main conduit for VEGF signaling (Ferrara, 2004; Holmes et al., 2007); however, heterodimers involving other VEGF receptors may also transduce a signal (Huang et al., 2001; Neagoe et al., 2005).

The structural details of the VEGF-VEGF receptor interaction have been gradually elucidated over the last dozen years. Domain deletion experiments have localized the VEGF binding site to domains 2 and 3, with domain 2 seeming to play a dominant role (Fuh et al., 1998; Lu et al., 2000). For Flt-1, domain 2 alone is necessary and sufficient for high-affinity binding, although domain 3 enhances affinity (Wiesmann et al., 1997). In contrast, KDR constructs lacking domain 3 bind VEGF weakly or not at all, but domain 2 is also required (Fuh et al., 1998; Lu et al., 2000). A crystal structure of a truncated form of VEGF (residues 8–109) bound to domain 2 of Flt-1 shows that the C terminus of domain 2 lies in a groove at one end of the VEGF dimer, suggesting that the beginning of domain 3 must be in close proximity (Wiesmann et al., 1997). A recent structure of KDR domains 2 and 3 bound to VEGF-C confirms this prediction,

showing the ligand bound at the interface between domains 2 and 3 (Leppänen et al., 2010). The detailed interactions between VEGF-C and KDR can, in many cases, serve as a model for the VEGF-A:KDR complex.

Given the importance of angiogenesis for cancer progression (Folkman, 1995), it is not surprising that an intense effort has been made to interfere with this process, and in particular with VEGF:KDR-mediated signaling, for the treatment of cancer (Ellis and Hicklin, 2008; Hsu and Wakelee, 2009). It is possible to block signal transduction via the VEGF receptors by inhibiting receptor tyrosine kinase activity; although ligand still binds the receptor, no signal is then sent to the rest of the cell (Ivy et al., 2009). Two such kinase inhibitors are on the market, namely sunitinib (Sutent; Pfizer) (Mendel et al., 2003), which is fairly specific to the VEGF and platelet-derived growth factor (PDGF) receptors (Roskoski, 2007a), and sorafenib (Nexavar; Bayer) (Wilhelm et al., 2004), which inhibits the VEGF receptors, PDGF receptors, and Raf (Wilhelm et al., 2008). It is also possible to prevent VEGF binding to KDR, by binding an interfering molecule to either the ligand or the receptor. Examples of the first approach include an anti-VEGF antibody such as bevacizumab (Avastin; Genentech) (Hurwitz et al., 2004) and a receptor mimic such as VEGF-Trap (Regeneron) (Holash et al., 2002). The second approach is exemplified by IMC-1121B (ramucirumab; ImClone Systems) and 6.64 (ImClone Systems), two antibodies directed against KDR (Lu et al., 2003; Witte et al., 1998).

IMC-1121B (hereafter shortened to "1121B") is very effective at blocking VEGF binding to KDR, as well as receptor phosphorylation and farther downstream signaling events (Miao et al., 2006). 1121B has demonstrated some antitumor efficacy in humans, including a decrease in tumor vascularity (Spratlin et al., 2010); additionally, a surrogate antibody directed against murine KDR inhibits angiogenesis (Prewett et al., 1999). Early on in the research effort that led to the (fully human) 1121B antibody, a murine anti-KDR antibody called "6.64" was identified as having VEGF-blocking ability (Lu et al., 2000). 6.64 was also shown to interfere with VEGF-mediated signaling pathways in the cell (Lu et al., 2003; Witte et al., 1998), but was not ultimately on the pathway that led to the tighter-binding and more effective 1121B. Both of these antibodies were shown to bind to KDR domain 3 exclusively, although they did not interfere with one another's binding (Lu et al., 2003).

We began this study hoping that a crystal structure of 1121B bound to KDR would explain the molecular mechanism by which 1121B interferes with VEGF signaling. In the course of determining this structure, we also solved the structure of 6.64 bound to KDR, and discovered that the two antibodies must block VEGF binding in two different ways, because it was hard to imagine how they could both occlude the same ligand binding site on KDR. We then carried out mutagenesis and binding experiments that have shown how both of these antibodies work to block VEGF signaling through KDR.

RESULTS

Structure Determination

In the course of determining the KDR d3:1121B Fab complex structure presented here, we also determined two other structures: the 1121B Fab fragment alone and the complex of KDR d3 with the Fab fragment of 6.64 (Table 1 and Figure 1; see Figure S1 available online). The 1121B structure was solved first to 2.2 Å, using the cetuximab Fab fragment from the cetuximab:EGFR structure (Li et al., 2005) as a molecular replacement search model. Separately, we determined the KDR d3:6.64 complex structure to 2.2 Å (Figure 1A) by molecular replacement with a structurally similar (but functionally unrelated) anticollagen Fab (Uysal et al., 2008); this partial solution provided clear enough electron density (Figure 1C) to allow us to build a model covering the entirety of KDR domain 3 (Figure 1D). Finally, we used the 1121B Fab and KDR domain 3 as molecular replacement search models to determine the KDR d3:1121B structure (Figure 1C) (a more detailed description of the structure determination can be found in Supplemental Experimental Procedures). The KDR d3:1121B complex crystallized in two space groups ($P4_32_12$ and $P3_221$) from the same growth condition, sometimes even from the same drop. We solved both structures, and found that the higher-resolution $P4_32_12$ structure has good electron density for the entire Fab and for the portion of KDR proximal to the Fab interface (Figure 1E); however, the density becomes less clear for the distal parts of KDR, probably due to a lack of stabilizing crystal contacts. The $P3_221$ complex (Figure 1B), despite its somewhat lower resolution, has good electron density for all of KDR domain 3, with a well-defined main chain and most side chains visible throughout the entire domain. Because the two structures are very similar (Cα root-mean-square deviation [rmsd] 1.2 Å over the entire complex, 0.8 Å considering only the KDR and Fv regions), we have used the $P3_221$ structure to look at the large-scale features of the complex, and the $P4_32_12$ structure to analyze the detailed antibody-receptor interactions.

The KDR d3:6.64 Complex

The structure of KDR domain 3, as seen in the KDR d3:6.64 complex, can be defined structurally as starting at Gly220 and ending at Pro328 (Figure 1D). The overall fold fits well in the class of Ig-like domains, with two antiparallel three- to four-stranded β sheets stacked in a sandwich. Our domain 3 structure is generally in excellent agreement with the recent structure of the KDR d2–d3:VEGF-C complex (Leppänen et al., 2010), with an overall Cα rmsd of 1.1 Å on domain 3 and only a few localized differences (see Discussion). The 6.64 Fab binds to a fairly extended area of KDR domain 3, mostly near the end of the domain containing the C terminus (Figures 2A and 2B). The Fab makes a few interactions with the very C-terminal end of our model; however, it should be noted that our domain 3 construct (KDR residues 220–338) is too long; it extends well past the domain 3-domain 4 boundary at residue 328, so residues 328–330 in our model are not in a biologically relevant conformation. All six of the 6.64 antibody complementarity-determining regions (CDRs) make interactions with KDR domain 3, including one close contact between Gly33 of the Fab light chain (amino acids in the 6.64 and KDR Fabs are numbered sequentially instead of by Kabat, Chothia, or other conventions) and one of the sugars in the N-glycosylation of KDR residue 245 (Figure 2A). The 6.64 binding epitope on KDR is highly discontinuous, with contacting residues scattered over five stretches of primary sequence (Figure 2B; see Figure S2A for a detailed list of contacts). A total of 982 $Å^2$ of solvent-accessible surface area on KDR domain 3 is buried in the 6.64 interface (residues 328–330 are excluded, as

Table 1. Data Collection and Refinement Statistics

	KDR:1121B Complex, Form 1		KDR:1121B Complex, Form 2		KDR:6.64 Complex		1121B Fab	
Data Collection Statistics								
Space group	$P4_32_12$		$P3_221$		$C222_1$		$P3_221$	
Unit cell (Å)	63.9, 63.9, 275.0		64.9, 64.9, 263.2		78.9, 112.1, 157.0		66.6, 66.6, 203.7	
Site of data collection	NSLS X4A		APS 31-ID (LRL-CAT)		APS 31-ID (LRL-CAT)		Home source	
Unique reflections	16,605		11,083		34,976		26,790	
Resolution (Å)	50–2.7	2.80–2.70	55–3.2	3.37–3.2	40–2.2	2.32–2.20	100–2.2	2.28–2.20
R_{sym}	0.106	0.553	0.099	0.688	0.124	0.619	0.060	0.219
Completeness (%)	99.8	99.1	98.6	98.8	98.2	97.7	97.5	78.7
Average redundancy	12.5	10.7	10.2	10.5	7.2	7.3	7.0	3.3
$I/\sigma(I)$	32.7	3.2	20.8	3.2	13.7	3.2	20.5	4.5
Refinement Statistics								
Resolution (Å)	50–2.7		55–3.2		40–2.2		70–2.2	
Reflections used (free)	15,653 (831)		10,548 (522)		33,185 (1,790)		25,334 (1,345)	
R factor	0.282		0.277		0.203		0.183	
R_{free}	0.315		0.332		0.259		0.223	
Rmsd								
Bonds (Å)	0.004		0.004		0.013		0.012	
Angles (°)	0.75		0.76		1.50		1.40	
Ramachandran statistics								
Most favored (%)	94.3		93.0		96.6		96.4	
Additional allowed (%)	5.5		6.8		3.0		3.4	
Outliers (%)	0.2		0.2		0.4		0.2	
Model contents								
Fab residues	430		429		434		429	
KDR residues	110		112		112		0	
Waters	0		0		375		257	
Other ligands					4 NAG, 6 Ca^{2+}		1 PO_4	
PDB ID code	3S37		3S36		3S35		3S34	

All four crystal forms have one molecule per asymmetric unit. APS, Advanced Photon Source; NSLS, National Synchrotron Light Source; NAG, N-acetylglucosamine; PO_4, phosphate ion.

they will be for all subsequent calculations), of which 55% is in the heavy-chain interface and 45% is in the light-chain interface. Including the Fab side of the interface, the total buried surface area is 2032 Å^2; for comparison, the buried surface area in the cetuximab:EGFR complex is 1770 Å^2 (Li et al., 2005), and in the bevacizumab:VEGF complex is about 1750 Å^2 (Muller et al., 1998).

The KDR d3:1121B Complex

The 1121B Fab binds to KDR domain 3 at the end of the domain closest to the N terminus (Figure 1B). This is almost diametrically opposite the binding site of 6.64 (Figure 1A), which validates the previous observation that 1121B and 6.64 do not compete with one another and can simultaneously bind to KDR (Lu et al., 2003). Gly220, the linker residue between KDR domains 2 and 3, is directly contacted by the Fab (Figures 2D and 2E), as are a number of residues in its vicinity. The 1121B binding epitope is much more localized than that of 6.64, consisting almost exclusively of a short β hairpin (KDR residues 312–317), an adjacent stretch of β strand (residues 251, 255, 257, 259, and 261), and the N terminus of domain 3 (residues 220–222) (Figures 2C–2E). The light chain of the 1121B Fab plays a fairly small role in this interaction, making a few hydrophobic contacts and one charge pair (between Lys92 of the light chain and Glu251 of KDR) (Figure 2E; detailed interactions can be found in Figure S2B). This asymmetry can also be seen in the buried solvent-accessible surface area: of the total 1001 Å^2 buried on KDR domain 3, 67% is in the heavy-chain interface and only 33% is in the light-chain interface. (The total buried area including the Fab is 1922 Å^2, somewhat less than for the 6.64 complex.) It should be noted, however, that the N terminus of KDR domain 3 points in the direction of the light-chain CDRs, and modeling based on the KDR:VEGF-C structure (Leppänen et al., 2010) indicates probable contacts between the light chain and KDR domain 2 (see Discussion).

The 1121B Fab fragment has changed conformation very little from the unbound structure to the KDR domain 3-bound structure. The elbow angle between variable and constant domains of the Fab has changed by less than 5°, and the Cα rmsd in the Fv region is only 0.46 Å, with some minor (<0.5 Å) rigid-body movements of the various CDRs. The only side-chain adjustment of note is a flip of Phe94 of the light chain

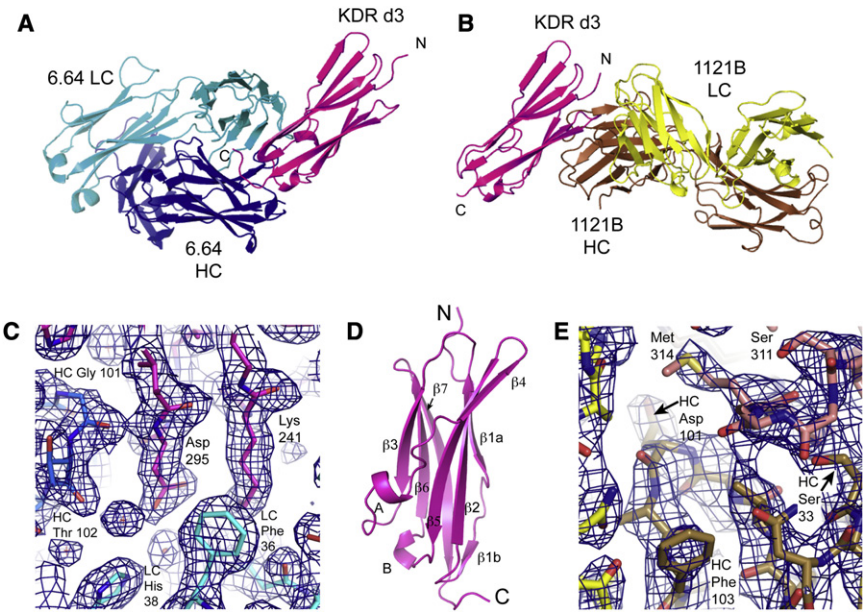

Figure 1. Structures of KDR Domain 3 Bound to 1121B and 6.64 Fabs

(A) Overview of the KDR:6.64 complex. A cartoon representation of the 6.64 Fab bound to domain 3 of KDR is shown with the Fab heavy chain in dark blue, the Fab light chain in light blue, and KDR domain 3 in magenta. The domain 3 N terminus is indicated at the upper right, and the C terminus is near the center of the image.

(B) Overview of the KDR:1121B complex. A cartoon representation of the 1121B Fab bound to KDR domain 3 is shown aligned so that the KDR portion superimposes on the KDR portion of the complex in (A). As above, KDR domain 3 is in magenta, while the 1121B Fab heavy chain is in dark yellow and the light chain is in light yellow. This color coding will be maintained in all subsequent figures.

(C) Electron density from the KDR:6.64 complex. A $2mF_o - DF_c$ map is shown as a blue mesh, contoured at 1 σ, in a region at the interface of KDR, the Fab heavy chain, and the Fab light chain. Selected residues from the three chains are labeled; LC indicates the Fab light chain, and HC indicates the Fab heavy chain.

(D) A cartoon view of KDR domain 3. Secondary-structure elements have been labeled, and the N and C termini are labeled for comparison with other figures.

(E) Electron density from the KDR:1121B complex, depicted as in (C). The Fab light chain is colored yellow, and is visible on the left side of the image.

See also Figure S1.

(the χ1 torsion angle goes from −82 in the unbound structure to 150 in the bound structure) to open up a pocket for Leu313 in the ligand (Figure 2E). Tyr57 and Tyr59 of the heavy chain, which are in that same area, have reoriented slightly to accommodate the bound KDR.

The structure of KDR domain 3 also seems not to be changed dramatically upon 1121B binding. In addition to the differences noted above versus the Leppänen et al. structure, the 6.64-bound and 1121B-bound structures can be compared against one another. In doing this analysis, we must keep in mind that the 1121B-bound structure is derived from the 6.64-bound structure; however, we think that our refinement is sufficiently robust that any model bias arising from the parental structure has been removed. The overall Cα rmsd between the 6.64- and 1121B-bound KDR structures is 0.51 Å. The most noticeable change in the 1121B-contacting portion of KDR domain 3 is a 1.5 Å movement of Met314 away from 1121B in order to relieve a steric clash with the main-chain oxygen of Thr100 on the heavy chain (Figure 1E). Met314 is pushed toward the rest of KDR domain 3, forcing a number of small shifts in the surrounding residues to accommodate it.

Mutagenesis and Binding Assays

To probe the functional importance of the residues involved in the 1121B and 6.64 binding interfaces, and to assess their contribution to VEGF binding, a series of alanine mutants was designed. Five of these mutants (M1–M5) were designed to cover small clusters of the primary sequence for ease of mutagenesis while blanketing the entire top (domain 2-proximal) surface of KDR domain 3 (Table 2 and Figures 3A and 3B). An additional two mutants (M6–M7) were designed along similar principles but were targeted to the 6.64 binding interface (Table 2 and Figures 3A and 3C). The final set of mutants targeted the KDR d2–d3 linker (M8), a patch on β strand 3 (M9), and the region of M1 (M1a–M1g) (Table 2; Table S1). All of the residues selected for alanine mutation are surface exposed and should not affect packing in the hydrophobic core of KDR domain 3. The first seven mutants (M1–M7) were expressed in constructs containing KDR domains 1–3 (residues 20–328, following the signal sequence) or domains 2–3 (residues 122–328), followed by an Fc fusion. The final set of mutants (M1a–M1g, M8, and M9) were expressed using the d2–3 construct only. It should be noted that these proteins are expressed and used in the assays as dimers, containing two copies of the KDR construct joined by disulfide links in their Fc tags. This dimeric receptor construct may bind VEGF more tightly than would an otherwise identical monomeric construct.

The mutant receptors were purified and assayed for binding to 1121B, 6.64, and VEGF-165. Binding data for d1–3 constructs M2–M7 and d2–3 M8 are shown in Figure 4 and Table 2; additional binding data for other d2–3 constructs is shown in Figure S3 and Table S1. Mutants M1 and M9 did not express at all in either the d1–3 or the d2–3 construct (Table S2); this may indicate a protein-folding defect in these mutants, even though the core of the domain is untouched. A series of follow-up mutants in the region of M1 identified one (M1a) that did not detectably bind either VEGF or 1121B (Figure S3 and Table S1); however, this mutant's low expression level (Table S2) and weak binding to 6.64 suggest that it, too, may have a folding problem in this region. The other constructs expressed robustly (Table S2). Mutant M5 severely affected 1121B binding, without altering the affinity for either 6.64 or VEGF. Conversely, mutant M7 abolished 6.64 binding completely, but had no effect on either 1121B or VEGF binding. Mutant M6 eliminated

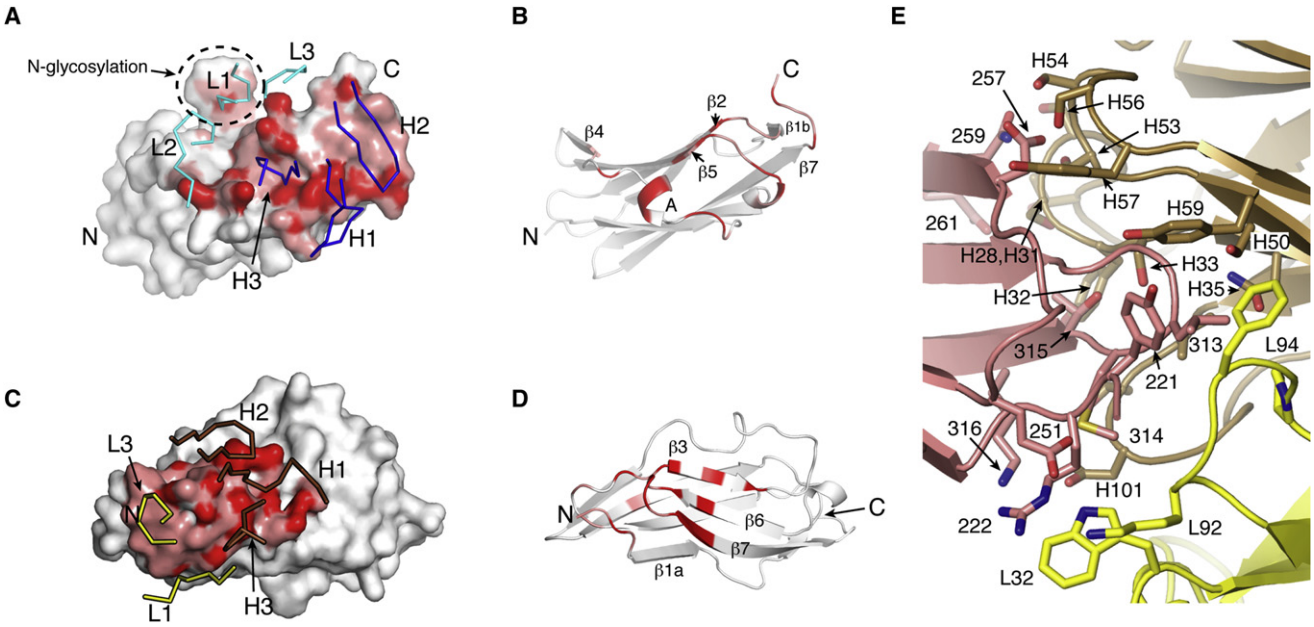

Figure 2. Details of the KDR-Antibody Interfaces

(A) Details of the KDR:6.64 interface. The molecular surface of KDR domain 3 is shown. Atoms which directly contact (<3.5 Å distance) an atom of the 6.64 Fab are colored red, while atoms which are close to the Fab (<5 Å distance) are colored pink. The six CDRs of the 6.64 Fab are shown as ribbons, colored as in Figure 1A. The large protrusion from the top center of the KDR surface in this view is one of the two N-glycosylations in the structure. The positions of the N and C termini of the KDR model are indicated.

(B) A cartoon view of KDR domain 3, in exactly the same orientation as (A). If any atom of a particular residue was colored red in (A), the backbone is colored red here. If an atom was colored pink (but none were red), the backbone is pink here. Selected secondary-structure elements are labeled.

(C) Details of the KDR:1121B interface. KDR domain 3 is depicted as in (A), but here shows interactions with the 1121B Fab. The CDRs of the Fab are shown, colored as in Figure 1C, except for CDR L2, which makes no contacts.

(D) A cartoon view equivalent to (B), but for the KDR:1121B interface. The orientation of (C) and (D) is related to that of (A) and (B) by an approximate 90° rotation about a horizontal axis.

(E) Details of the KDR d3:1121B interface. The backbones of KDR and 1121B are shown in cartoon representation, with KDR d3 colored pink, the 1121B light chain in yellow, and the 1121B heavy chain in brown. Side chains which form interactions between KDR and 1121B are shown in stick form. KDR residues are identified by residue number only, while 1121B heavy-chain residues have the prefix "H" and light-chain residues have the prefix "L."

See Figure S2 for another depiction of the KDR-1121B contacts.

binding to 6.64, but also reduced affinity for 1121B and VEGF; this mutant may also have destabilized the structure of the KDR domain. Finally, mutant M2 shows a lower affinity for VEGF without appreciably affecting the binding to 1121B or to 6.64.

To further understand the relationships between the two antibody binding sites and the VEGF binding site, we tested 1121B and 6.64 for their ability to block KDR binding to VEGF. We examined three KDR constructs: the d1–3-Fc construct described above, a d1–7-AP fusion used in our previous work (Lu et al., 2000), and a commercially available d1–7-Fc fusion. Like the Fc fusions, the AP fusion protein is dimeric in solution, and the three proteins have similar affinities for the two antibodies and for VEGF (Table 2). However, the blocking behavior is very different. 1121B blocks VEGF binding to all three constructs with roughly similar affinity (Figure 5A); the higher EC_{50} for blocking the d1–7-Fc fusion can be explained by the higher affinity this fusion has for VEGF (Table 2). The blocking ability of 6.64, however, is almost completely eliminated with the Fc fusions (Figure 5B), despite the fact that 6.64 binds to these constructs with nearly the same affinity as it does to d1–7-AP (Table 2).

DISCUSSION

The most striking feature of the KDR:1121B structure compared to the KDR:6.64 structure is how the two Fabs bind almost at opposite poles of KDR domain 3, with 1121B at the domain 2-proximal end and 6.64 at the domain 4-proximal end (Figure 6A). The binding surfaces of the two Fabs do not overlap at all (Figure 2), suggesting that both antibodies could even bind simultaneously to the same molecule of KDR. This is consistent with previous data showing that KDR, even when fully saturated with one of these two antibodies, still has room to bind the other (Lu et al., 2003). The disjunction of the two antibody binding epitopes raises the question: how can both of these antibodies interfere with VEGF binding to KDR?

Thanks to the recently published structure of VEGF-C bound to KDR domains 2 and 3 (Leppänen et al., 2010), we have a much clearer picture of how 1121B and 6.64 work as VEGF blockers. This structure is not a perfect model for the VEGF-A:KDR complex, because there are small but significant differences in the relative orientation of the ligand and domain 2 of the receptor when compared to the Flt-1 domain 2:VEGF-A crystal structure (Wiesmann et al., 1997). However, it serves for

Table 2. KDR Mutant Binding Constants

KDR Construct	Mutation	Binding K_D (nM) 1121B Fab	6.64 Fab	VEGF
d1–7-AP	Wild-type	0.070	0.30	2.42
d1–7-Fc	Wild-type	0.113	0.97	0.20
d1–3-Fc	Wild-type	0.056	0.36	2.28
d2–3-Fc	Wild-type	0.057	0.58	3.25
d1–3 M1	^{220}GYRIYD→AAAIAA	nd	nd	nd
d1–3 M2	^{251}ELN→AAA	0.133	0.80	23.3
d1–3 M3	^{278}KTQS→AAAA	0.086	1.30	1.89
d1–3 M4	^{282}GSEMKK→AAEAKA	0.090	1.05	1.71
d1–3 M5	^{312}GLMTK→AAATA	28.0	1.15	1.69
d1–3 M6	^{238}VGEKLV→AAAALA	0.223	2.52	2.80
d1–3 M7	^{295}DGVTR→AAVAA	0.089	nb	1.07
d2–3 M8	^{217}VVVG→AAAA	0.084	0.52	7.12
d2–3 M9	^{255}GIDFN→AIAFA	nd	nd	nd

nb, no detectable binding; nd, binding not determined because construct did not express.

the purpose at hand. A superposition of the KDR:1121B structure onto the KDR:VEGF-C structure reveals that there is an overlap in the position of a loop in VEGF-C (residues 189–194) and CDR H2 (residues 57–59) of 1121B (Figure 6B). This loop is two residues shorter in VEGF-A, which is not enough to relieve the steric clash, and it is highly unlikely that either the VEGF or the 1121B structure could be distorted to avoid the overlap without a substantial energetic penalty. We also observe some steric interference between KDR domain 2 and the light chain of 1121B (Figure 6A). Although this clash could be relieved by a fairly small motion of domain 2, that same motion would alter the VEGF binding site, perhaps to a degree incompatible with VEGF binding. Therefore, 1121B blocks VEGF signaling in two ways: by sterically preventing the ligand from binding to KDR, and by changing the receptor conformation so that it cannot bind ligand.

The mechanism of 6.64 action is less obvious. When the KDR:6.64 structure is superimposed onto the KDR:VEGF-C structure, there is no overlap between the antibody and the VEGF; the closest pair of Cα atoms is about 15 Å apart. Therefore, 6.64 is not a direct blocker like 1121B. 6.64 does not appear to sterically prevent receptor dimerization in the manner of pertuzumab (Franklin et al., 2004), because a dimeric Fab:receptor:ligand model can be constructed with no overlaps (Figure 6C). It is possible that 6.64 binding could cause a conformational change in KDR domain 3 that prevents VEGF binding. However, comparison of our 6.64-bound and 1121B-bound structures (see above) showed no differences likely to affect VEGF binding. We did observe a difference when comparing our structures to the KDR d2–d3:VEGF-C structure (Leppänen et al., 2010) in the area of residues 268–282. In the Leppänen et al. structure, this region is a fairly simple β strand formed by residues 269–276, with a large loop connecting it to the β strand we are calling β5 (Figure 1D). In our structure, by contrast, residues 268–272 form one turn of an α helix, followed by a bulged β strand in which residues 278–282 are offset by two positions from their locations in the Leppänen et al. structure (Figure S1B). Two of the residues in this area, Lys271 and Arg275, make contacts with the 6.64 Fab, so it is possible that Fab binding has induced this change. We think this is unlikely because our 1121B-bound structure looks the same as the 6.64-bound structure in this region, and because Leppänen et al. note that this portion of their structure

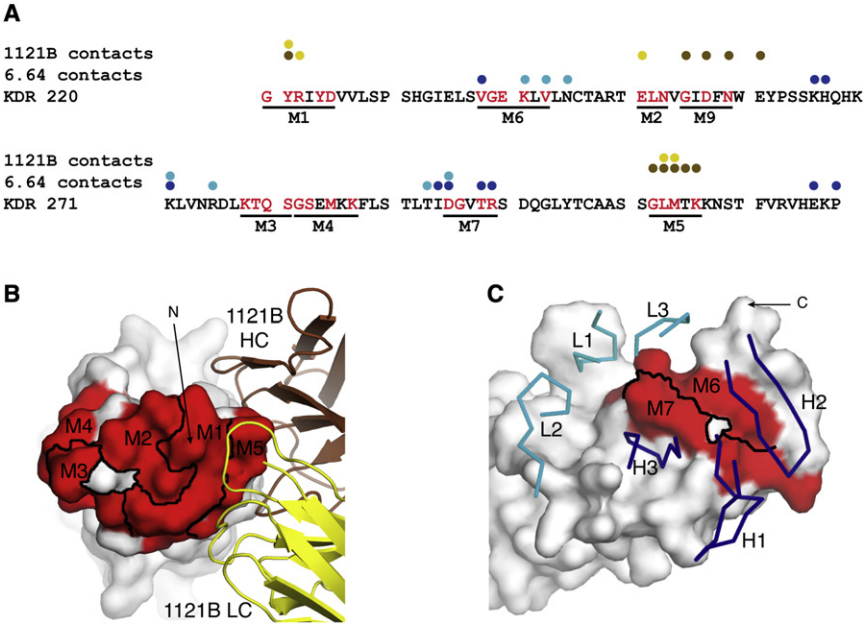

Figure 3. A Schematic of the KDR Mutagenesis

(A) The sequence of KDR domain 3 is shown, with the residues involved in mutants M1–M7 and M9 colored red. Residues contacting the 1121B light chain have a yellow dot above them, while residues contacting the 1121B heavy chain have a brown dot above them; if a residue contacts both chains of the Fab, it has both dots above it. Similarly, light blue and dark blue dots are used to indicate contacts to the 6.64 light and heavy chains, respectively. See Figure S2 for a detailed list of antibody-KDR contacts.

(B) The top (domain 2-proximal) surface of KDR domain 3 is shown, with the N terminus indicated. Residues colored red were mutated to alanine; the surface patches corresponding to particular mutants are delineated by black lines. The two uncolored patches in the middle of the surface correspond to main-chain atoms of unmutated (hydrophobic core) residues. The bound 1121B Fab is shown in cartoon representation.

(C) The surface of KDR domain 3 is shown in the same orientation as Figure 2A, with the 6.64 CDRs drawn as thin Cα traces for reference. The red surface corresponds to mutants M6 and M7, separated by the black line as indicated.

See also Table S2 for KDR mutant expression levels.

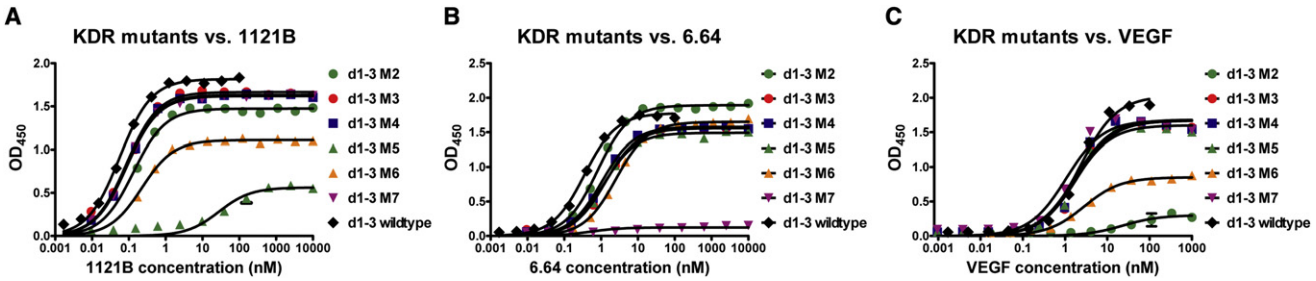

Figure 4. KDR Mutant Binding ELISAs

Binding curves to 1121B Fab (A), 6.64 Fab (B), and VEGF-165 (C) are shown for KDR d1–3 mutants M2–M7 and d1–3 wild-type. Points and error bars represent mean ± SEM of duplicate or triplicate measurements. Curves are nonlinear fits to a single-site binding equation. See Figure S3 and Table S1 for additional KDR mutant binding data.

is poorly ordered. In any event, none of the residues in question here make contacts to bound VEGF-C (Leppänen et al., 2010).

One possible mechanism of 6.64 action is suggested by our observation that 6.64 blocking of Fc-tagged KDR d1–3 or d1–7 is far weaker than its blocking of d1–7-AP, even though the antibody binding affinity to these three proteins is quite similar. Our structure shows that 6.64 binds near the domain 3:domain 4 interface, and there is reason to think that domain 4 is involved in KDR dimerization, both from analogy with c-Kit (Yuzawa et al., 2007) and from electron microscopy of dimeric KDR:VEGF complexes (Ruch et al., 2007). Even if bound 6.64 cannot sterically interfere with receptor dimerization, the altered receptor conformation could be an indirect interference producing the same net result. The AP fusion of KDR domains 1–7, unlike the two Fc fusions tested, does not have a covalent link between the two monomers. This raises the possibility that antibody binding could dissociate the receptor dimer completely, explaining the enhanced blocking affinity of 6.64 against d1–7-AP (Figure 5B). Because 6.64 is known to be effective at blocking VEGF signaling in cells (Witte et al., 1998), it seems that in this case the d1–7-AP fusion is better than the Fc fusion at mimicking the naturally occurring receptor dimer.

We designed our KDR mutants without knowledge of the KDR:VEGF-C structure, in order to map the VEGF binding site; however, they can also serve to test which residues contacting VEGF-C are functionally important for binding VEGF-A. We observed that mutant M5 (at the center of the 1121B binding interface) eliminated 1121B binding without affecting 6.64 binding, whereas mutant M7 (in the 6.64 interface) had the reverse effect, showing that the antibody epitopes are functionally as well as structurally separate. Neither of these mutants affected VEGF binding; although Gly312 (changed to Ala in mutant M5) is fairly close to Pro191 in VEGF-C, this contact is too peripheral to be important for ligand binding. Mutant M2, in contrast, targets residues in the middle of the VEGF-C interface, in particular Leu252 and Asn253, and this mutant has a dramatic effect on VEGF binding (Figure 4C). Mutant M8, in the linker between KDR domains 2 and 3, had a modest effect on VEGF binding, smaller than the 8-fold drop seen by Leppänen et al. when they replaced this sequence with the corresponding sequence from VEGFR1. It seems likely that this region, which is contacted by hydrophobic residues in VEGF-A and VEGF-C, needs only to be hydrophobic. Mutation from valine to alanine is thus less disruptive than changing to the hydrophilic VEGFR1 sequence.

In conclusion, our structures of 1121B and 6.64 bound to KDR domain 3 have shown two different ways to interfere with ligand-receptor binding. 1121B acts in the classic way, by sterically preventing VEGF from reaching its binding interface on the receptor. Interestingly, 1121B can do this even though not a single residue on KDR directly contacts both 1121B and VEGF-C. The fact that the binding sites are immediately adjacent, and that the 1121B and VEGF-C molecules extend beyond their footprints on the KDR surface, is enough to induce the steric overlap that prevents VEGF binding in the presence of 1121B. 6.64, by contrast, appears to work more indirectly, perhaps by rearranging the domain 3:domain 4 interface of KDR in such a way that the receptor can no longer dimerize. These modes of action are not mutually exclusive: cetuximab binds to EGF receptor in a way that blocks ligand binding and at the same time prevents the receptor from adopting a conformation that would allow dimerization and signaling (Li et al., 2005). These structures show the multiple ways that an antibody drug can achieve its clinical goal: disrupting a signaling pathway necessary for the growth or survival of a cancer cell.

Significance

Inhibition of angiogenesis is an important strategy in treating many diseases, from macular degeneration to cancer. A number

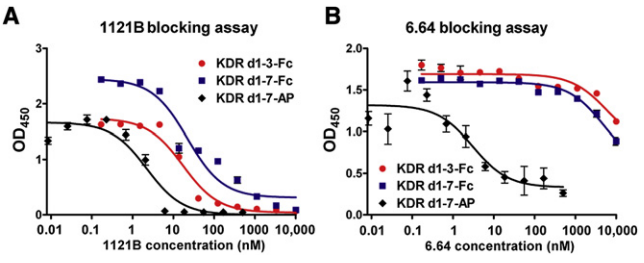

Figure 5. KDR-Blocking ELISAs

(A) 1121B Fab blocking the binding of KDR d1–3-Fc, d1–7-Fc, or d1–7-AP to VEGF-165. Points and error bars represent mean ± SEM of duplicate or triplicate measurements. Curves are nonlinear fits to a single-site inhibition equation, with fixed K_D and concentration for the KDR-VEGF interaction as described in Experimental Procedures.

(B) As in (A), but showing 6.64 Fab blocking.

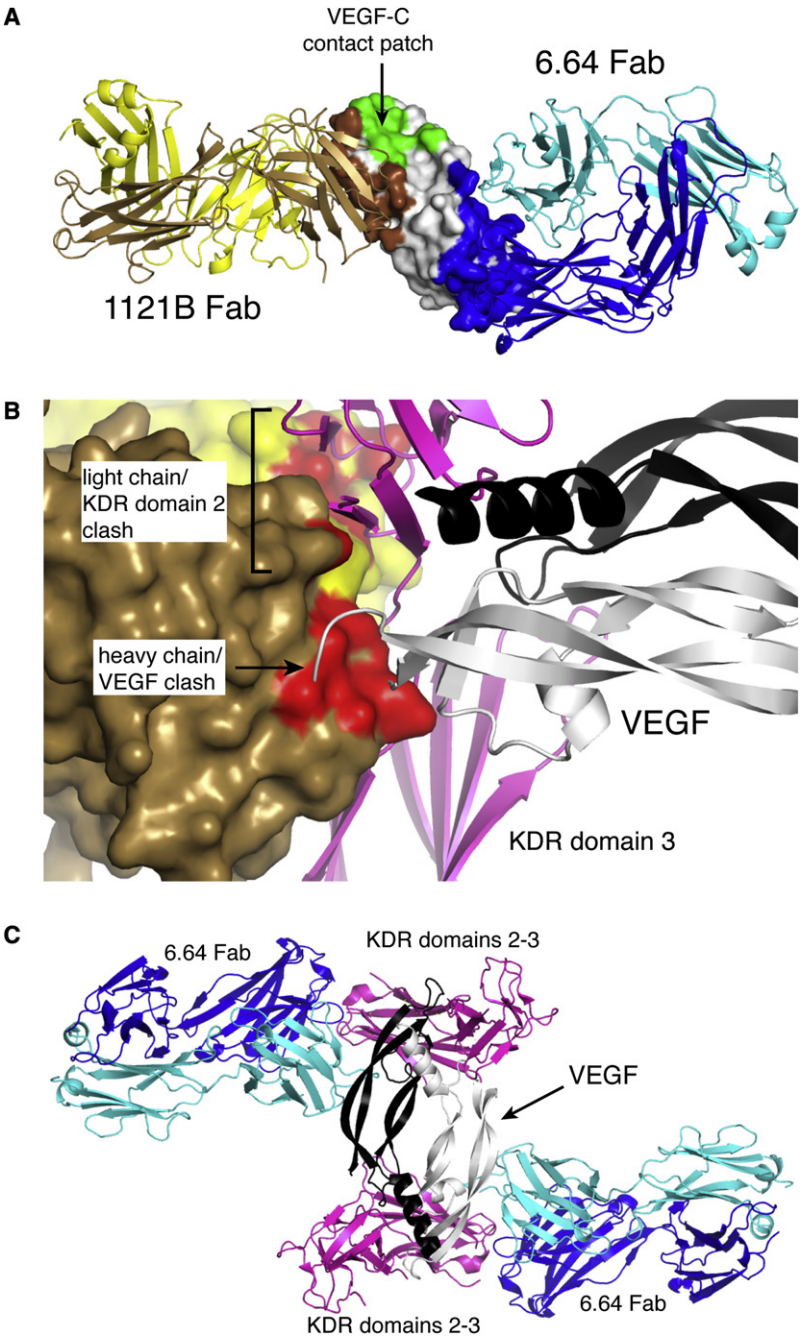

Figure 6. Mechanism of Action of 1121B and 6.64

(A) Binding of 1121B, 6.64, and VEGF to KDR domain 3. The KDR:1121B and KDR:6.64 structures have been superimposed on their common KDR domain 3. KDR domain 3 from the KDR:6.64 complex is shown in surface representation, while the superimposed 1121B and 6.64 Fabs are shown in cartoon representation, colored as in Figure 1. The contact patches (corresponding to the pink and red coloring in Figure 2) are shown in brown for 1121B and blue for 6.64. Additionally, the contact patch of VEGF-C (Leppänen et al., 2010) is shown in green.

(B) Steric clash between 1121B and VEGF. The KDR d2–d3:VEGF-C structure (Leppänen et al., 2010) is shown in cartoon representation, with KDR colored magenta and the two chains of VEGF-C colored black and white. The superimposed KDR:1121B structure is shown with the Fab in surface representation, colored as in Figure 1B. The red patch in the foreground on the surface of 1121B represents those atoms within 2.2 Å of an atom in VEGF-C. Additional red patches in the background indicate 1121B atoms within 2.2 Å of an atom in the superimposed KDR domain 2.

(C) Noninterference of 6.64 with the KDR:VEGF dimer. The full dimer of KDR d2–d3 bound to VEGF-C (Leppänen et al., 2010) is shown in cartoon representation, colored as in (B), while two copies of the 6.64 Fab, colored as in Figure 1A, are superimposed on each copy of KDR domain 3.

of anticancer therapies have focused on disrupting the signaling pathway involving vascular endothelial growth factors (VEGFs) and their receptors, in particular VEGF receptor 2, or KDR. One such therapy is a fully human anti-KDR antibody called IMC-1121B, currently in phase III clinical trials. Our structure of the Fab fragment of IMC-1121B in complex with domain 3 of KDR reveals the molecular mechanism by which this antibody prevents angiogenic signaling through KDR. This antibody prevents all VEGF family ligands from binding to this receptor, and has great promise as a broadly effective antiangiogenic cancer therapy.

EXPERIMENTAL PROCEDURES

See Supplemental Experimental Procedures for more details on everything described below.

6.64 and 1121B Fab Production

1121B Fab was expressed and purified as previously described (Miao et al., 2006). 6.64 Fab was cloned into the mammalian expression pEE6.1 and pEE14.1 (Lonza Biologics) and expressed in human 293 FreeStyle cells (Invitrogen) by transient transfection. 6.64 Fab was purified from conditioned media by a multistep purification including two passes over an SP-Sepharose HP column (GE Healthcare) and one pass over a Superdex-200 column (GE Healthcare).

KDR Protein Production

KDR domain 3, containing residues Gly220–Ser328 of human KDR with an N-terminal His tag, was expressed in Hi5 insect cells (Novagen) and purified from conditioned media by an Ni Sepharose HP column (GE Healthcare) followed by a Superdex-200 column. The His tag was then removed using factor Xa, and the KDR domain 3 was repurified by the Superdex-200 column. For the mutagenesis work, two KDR constructs, containing residues 20–328 (domains 1–3) or residues 122–328 (domains 2–3) of human KDR, were cloned into a proprietary mammalian expression vector that produces the resulting protein with a C-terminal Fc tag and an N-terminal CMV secretion signal sequence. These wild-type proteins, and the mutants derived from them, were expressed in 293 FreeStyle cells by transient transfection, and then purified from conditioned media by binding to a small protein A column, elution with Gentle Elution Buffer (Pierce), and desalting using a PD-10 column (GE Life Sciences).

Crystallization and Structure Determination

Purified KDR domain 3 was mixed with either the 6.64 Fab or the 1121B Fab, with a slight molar excess of KDR, and allowed to incubate overnight at 4°C.

The complex was then purified away from excess KDR by a Superdex-200 gel filtration column (GE Healthcare) and concentrated to 15–20 mg/ml for crystallization trials. The concentrated crystallization stock was in 50 mM Tris (pH 8), 250 mM NaCl. Crystals were grown by hanging- and sitting-drop vapor diffusion, with the protein stock mixed 1:1 with the well solution. For the KDR:6.64 complex crystals, the best well solution was 0.1 M $CdCl_2$, 0.1 M Na acetate (pH 4.6), 30% (v/v) PEG 400. For the KDR:1121B complex crystals, the best well solution was 0.1 M imidazole (pH 6.5), 0.1 M $CaCl_2$, 40% (w/v) PEG 1500, 10% (v/v) isopropanol. The KDR:1121B crystallization condition produced two different crystal forms, one with space group $P3_221$ and one with space group $P4_32_12$ (see below); both forms would sometimes be present in the same drop. Crystals of 1121B Fab alone were grown in 100 mM sodium/potassium phosphate (pH 5.5), 40% (v/v) PEG 400. All of these crystals could be frozen in liquid nitrogen directly from the mother liquor due to the PEG 400 or isopropanol acting as a cryostabilizer. Data for the KDR:6.64 crystals and for the KDR:1121B crystals ($P3_221$ form) were collected at the LRL-CAT beamline (31-ID) at the Advanced Photon Source, Argonne National Laboratory. Data for the KDR:1121B crystals ($P4_32_12$ form) were collected at beamline X4C at the National Synchrotron Light Source, Brookhaven National Laboratory. Data for the 1121B Fab crystals were collected on our home X-ray source, a Rigaku MicroMax 007HF with Saturn-944 CCD detector. Data statistics can be found in Table 1.

The 1121B Fab structure was solved by molecular replacement using Phaser (McCoy et al., 2007), with the Fab fragment of cetuximab from the cetuximab:EGFR structure (Protein Data Bank [PDB] ID code 1YY9) (Li et al., 2005) as a search model. An initial solution for the KDR:6.64 structure was also found by molecular replacement with search models of the Fab constant and variable domains from PDB ID code 2VL5 (Uysal et al., 2008), chosen because it is also a mouse IgG1 antibody. The KDR domain 3 in this complex could not be found by molecular replacement; however, the electron density was of sufficient quality to allow the molecule to be built by hand. The KDR domain 3 model was refined using Refmac (Murshudov et al., 1997) over several rounds, with TLS refinement and automatic water picking. The final model contains all residues of KDR domain 3 from 220 to 328, plus one proline at the N terminus from the factor Xa cleavage site.

The Fab portion of the KDR:1121B complex was found by molecular replacement using the refined 1121B Fab structure as a search model, whereas the KDR portion was found using the refined KDR domain 3 structure from the KDR:6.64 complex. This solution, containing heavy and light chains of the 1121B Fab as well as KDR domain 3, was refined with Refmac, using limited TLS refinement and tight geometric restraints to prevent overfitting. Some manual rebuilding of the Fab and KDR structures was necessary, especially in the area of the Fab:KDR interface, but we left most of the structure as it was in the high-resolution models unless difference electron density clearly defined an alternate position.

Binding and Blocking ELISAs

Binding ELISAs were performed by coating KDR d1-3-Fc wild-type, and the mutants derived from it, on the surface of Immulon 2 HB plates (Thermo Scientific), blocking, washing, and then applying serial dilutions of the appropriate binding partner (VEGF-165, 1121B Fab, or 6.64 Fab) and incubating at room temperature for 1 hr. Secondary antibodies were matched to the binding partner: for 6.64, 1121B, and VEGF, these were goat anti-mouse light chain (Jackson ImmunoResearch), anti-human light chain (Jackson ImmunoResearch), and anti-VEGF polyclonal (R&D Systems), all of which were HRP conjugated.

For the blocking ELISA, VEGF-165 was coated overnight on Immulon 2 HB plates; the plates were then blocked and washed. Separately, serial dilutions of 1121B Fab or 6.64 Fab were prepared in a solution containing phosphate-buffered saline, 0.05% Tween-20, 1% milk powder, and 1 ng/μl KDR (this corresponds to about 6.7 nM d1–7-AP, 9.1 nM d1–7-Fc, and 16 nM d1–3-Fc) and then incubated for 1 hr at room temperature prior to addition to the plate. The Fab:KDR mixtures were then added to the plates and incubated for a further hour at room temperature, after which the plates were washed, incubated with secondary antibody (HRP-conjugated anti-human Fc [Jackson ImmunoResearch] for the Fc-tagged constructs, or His-Probe [Thermo Scientific] for the AP construct, which also has a His tag), and developed. K_i values were determined using the single-site K_i model in GraphPad Prism (GraphPad Software), with the concentrations of the "hot" ligands (the KDR constructs) input as listed above, and the binding constants of the "hot" ligands to VEGF (determined from other ELISAs) input as 2.4, 0.2, and 2.3 nM for d1–7-AP, d1–7-Fc, and d1–3-Fc, respectively.

ACCESSION NUMBERS

The structures of the 1121B Fab alone and of the KDR d3:6.64 complex have been deposited in the Protein Data Bank under ID codes 3S34 and 3S35, respectively. The structures of the KDR d3:1121B complex in $P3_221$ and $P4_32_12$ crystal forms have been deposited under PDB ID codes 3S36 and 3S37, respectively.

SUPPLEMENTAL INFORMATION

Supplemental Information includes Supplemental Experimental Procedures, three figures, and two tables and can be found with this article online at doi:10.1016/j.str.2011.01.019.

ACKNOWLEDGMENTS

We thank Jaafar Sleiman Haidar, Yang Shen, Nabil Chehab, John Haurum, and Larry Witte for their comments on the manuscript. Use of the National Synchrotron Light Source, Brookhaven National Laboratory, was supported by the U.S. Department of Energy, Office of Science, Office of Basic Energy Sciences, under contract DE-AC02-98CH10886. Use of the Advanced Photon Source at Argonne National Laboratory was supported by the U.S. Department of Energy, Office of Science, Office of Basic Energy Sciences, under contract DE-AC02-06CH11357. KDR domain 3 was cloned and expressed by S.P., E.C.N., and Y.W. 6.64 Fab was cloned by P.S., expressed by K.P. and A.B., and purified by L.S. KDR domain 3 and 1121B Fab were purified by M.C.F., E.C.N., Y.W., and S.P. Crystals were grown by M.C.F., E.C.N., and Y.W. Data collection and structure determination were done by M.C.F. KDR mutants were cloned by Y.Z., expressed by K.P. and A.B., and purified by M.C.F. and H.G. ELISAs were performed by M.C.F. The manuscript and figures were prepared by M.C.F. and P.K. All of the authors are employees of ImClone Systems (a wholly owned subsidiary of Eli Lilly and Company), which makes IMC-1121B and is currently evaluating it in clinical trials.

Received: September 28, 2010
Revised: January 10, 2011
Accepted: January 23, 2011
Published: August 9, 2011

REFERENCES

Chua, R.A., and Arbiser, J.L. (2009). The role of angiogenesis in the pathogenesis of psoriasis. Autoimmunity *42*, 574–579.

de Vries, C., Escobedo, J.A., Ueno, H., Houck, K., Ferrara, N., and Williams, L.T. (1992). The fms-like tyrosine kinase, a receptor for vascular endothelial growth factor. Science *255*, 989–991.

Ellis, L.M., and Hicklin, D.J. (2008). VEGF-targeted therapy: mechanisms of anti-tumour activity. Nat. Rev. Cancer *8*, 579–591.

Ferrara, N. (2004). Vascular endothelial growth factor: basic science and clinical progress. Endocr. Rev. *25*, 581–611.

Folkman, J. (1995). Angiogenesis in cancer, vascular, rheumatoid and other disease. Nat. Med. *1*, 27–31.

Franklin, M.C., Carey, K.D., Vajdos, F.F., Leahy, D.J., de Vos, A.M., and Sliwkowski, M.X. (2004). Insights into ErbB signaling from the structure of the ErbB2-pertuzumab complex. Cancer Cell *5*, 317–328.

Fuh, G., Li, B., Crowley, C., Cunningham, B., and Wells, J.A. (1998). Requirements for binding and signaling of the kinase domain receptor for vascular endothelial growth factor. J. Biol. Chem. *273*, 11197–11204.

Grassot, J., Gouy, M., Perrière, G., and Mouchiroud, G. (2006). Origin and molecular evolution of receptor tyrosine kinases with immunoglobulin-like domains. Mol. Biol. Evol. *23*, 1232–1241.

Hiratsuka, S., Minowa, O., Kuno, J., Noda, T., and Shibuya, M. (1998). Flt-1 lacking the tyrosine kinase domain is sufficient for normal development and angiogenesis in mice. Proc. Natl. Acad. Sci. USA *95*, 9349–9354.

Holash, J., Davis, S., Papadopoulos, N., Croll, S.D., Ho, L., Russell, M., Boland, P., Leidich, R., Hylton, D., Burova, E., et al. (2002). VEGF-Trap: a VEGF blocker with potent antitumor effects. Proc. Natl. Acad. Sci. USA *99*, 11393–11398.

Holmes, K., Roberts, O.L., Thomas, A.M., and Cross, M.J. (2007). Vascular endothelial growth factor receptor-2: structure, function, intracellular signalling and therapeutic inhibition. Cell. Signal. *19*, 2003–2012.

Hsu, J.Y., and Wakelee, H.A. (2009). Monoclonal antibodies targeting vascular endothelial growth factor: current status and future challenges in cancer therapy. BioDrugs *23*, 289–304.

Huang, K., Andersson, C., Roomans, G.M., Ito, N., and Claesson-Welsh, L. (2001). Signaling properties of VEGF receptor-1 and -2 homo- and heterodimers. Int. J. Biochem. Cell Biol. *33*, 315–324.

Hurwitz, H., Fehrenbacher, L., Novotny, W., Cartwright, T., Hainsworth, J., Heim, W., Berlin, J., Baron, A., Griffing, S., Holmgren, E., et al. (2004). Bevacizumab plus irinotecan, fluorouracil, and leucovorin for metastatic colorectal cancer. N. Engl. J. Med. *350*, 2335–2342.

Ivy, S.P., Wick, J.Y., and Kaufman, B.M. (2009). An overview of small-molecule inhibitors of VEGFR signaling. Nat. Rev. Clin. Oncol. *6*, 569–579.

Kaipainen, A., Korhonen, J., Mustonen, T., van Hinsbergh, V.W., Fang, G.H., Dumont, D., Breitman, M., and Alitalo, K. (1995). Expression of the fms-like tyrosine kinase 4 gene becomes restricted to lymphatic endothelium during development. Proc. Natl. Acad. Sci. USA *92*, 3566–3570.

Leppänen, V.M., Prota, A.E., Jeltsch, M., Anisimov, A., Kalkkinen, N., Strandin, T., Lankinen, H., Goldman, A., Ballmer-Hofer, K., and Alitalo, K. (2010). Structural determinants of growth factor binding and specificity by VEGF receptor 2. Proc. Natl. Acad. Sci. USA *107*, 2425–2430.

Li, S., Schmitz, K.R., Jeffrey, P.D., Wiltzius, J.J., Kussie, P., and Ferguson, K.M. (2005). Structural basis for inhibition of the epidermal growth factor receptor by cetuximab. Cancer Cell *7*, 301–311.

Lu, D., Kussie, P., Pytowski, B., Persaud, K., Bohlen, P., Witte, L., and Zhu, Z. (2000). Identification of the residues in the extracellular region of KDR important for interaction with vascular endothelial growth factor and neutralizing anti-KDR antibodies. J. Biol. Chem. *275*, 14321–14330.

Lu, D., Shen, J., Vil, M.D., Zhang, H., Jimenez, X., Bohlen, P., Witte, L., and Zhu, Z. (2003). Tailoring in vitro selection for a picomolar affinity human antibody directed against vascular endothelial growth factor receptor 2 for enhanced neutralizing activity. J. Biol. Chem. *278*, 43496–43507.

McCoy, A.J., Grosse-Kunstleve, R.W., Adams, P.D., Winn, M.D., Storoni, L.C., and Read, R.J. (2007). Phaser crystallographic software. J. Appl. Crystallogr. *40*, 658–674.

Mendel, D.B., Laird, A.D., Xin, X., Louie, S.G., Christensen, J.G., Li, G., Schreck, R.E., Abrams, T.J., Ngai, T.J., Lee, L.B., et al. (2003). In vivo antitumor activity of SU11248, a novel tyrosine kinase inhibitor targeting vascular endothelial growth factor and platelet-derived growth factor receptors: determination of a pharmacokinetic/pharmacodynamic relationship. Clin. Cancer Res. *9*, 327–337.

Meyer, R.D., Mohammadi, M., and Rahimi, N. (2006). A single amino acid substitution in the activation loop defines the decoy characteristic of VEGFR-1/FLT-1. J. Biol. Chem. *281*, 867–875.

Miao, H.Q., Hu, K., Jimenez, X., Navarro, E., Zhang, H., Lu, D., Ludwig, D.L., Balderes, P., and Zhu, Z. (2006). Potent neutralization of VEGF biological activities with a fully human antibody Fab fragment directed against VEGF receptor 2. Biochem. Biophys. Res. Commun. *345*, 438–445.

Muller, Y.A., Chen, Y., Christinger, H.W., Li, B., Cunningham, B.C., Lowman, H.B., and de Vos, A.M. (1998). VEGF and the Fab fragment of a humanized neutralizing antibody: crystal structure of the complex at 2.4 Å resolution and mutational analysis of the interface. Structure *6*, 1153–1167.

Murshudov, G.N., Vagin, A.A., and Dodson, E.J. (1997). Refinement of macromolecular structures by the maximum-likelihood method. Acta Crystallogr. D Biol. Crystallogr. *53*, 240–255.

Neagoe, P.E., Lemieux, C., and Sirois, M.G. (2005). Vascular endothelial growth factor (VEGF)-A165-induced prostacyclin synthesis requires the activation of VEGF receptor-1 and -2 heterodimer. J. Biol. Chem. *280*, 9904–9912.

Pajusola, K., Aprelikova, O., Korhonen, J., Kaipainen, A., Pertovaara, L., Alitalo, R., and Alitalo, K. (1992). FLT4 receptor tyrosine kinase contains seven immunoglobulin-like loops and is expressed in multiple human tissues and cell lines. Cancer Res. *52*, 5738–5743.

Park, J.E., Chen, H.H., Winer, J., Houck, K.A., and Ferrara, N. (1994). Placenta growth factor. Potentiation of vascular endothelial growth factor bioactivity, in vitro and in vivo, and high affinity binding to Flt-1 but not to Flk-1/KDR. J. Biol. Chem. *269*, 25646–25654.

Prewett, M., Huber, J., Li, Y., Santiago, A., O'Connor, W., King, K., Overholser, J., Hooper, A., Pytowski, B., Witte, L., et al. (1999). Antivascular endothelial growth factor receptor (fetal liver kinase 1) monoclonal antibody inhibits tumor angiogenesis and growth of several mouse and human tumors. Cancer Res. *59*, 5209–5218.

Roskoski, R., Jr. (2007a). Sunitinib: a VEGF and PDGF receptor protein kinase and angiogenesis inhibitor. Biochem. Biophys. Res. Commun. *356*, 323–328.

Roskoski, R., Jr. (2007b). Vascular endothelial growth factor (VEGF) signaling in tumor progression. Crit. Rev. Oncol. Hematol. *62*, 179–213.

Roskoski, R., Jr. (2008). VEGF receptor protein-tyrosine kinases: structure and regulation. Biochem. Biophys. Res. Commun. *375*, 287–291.

Ruch, C., Skiniotis, G., Steinmetz, M.O., Walz, T., and Ballmer-Hofer, K. (2007). Structure of a VEGF-VEGF receptor complex determined by electron microscopy. Nat. Struct. Mol. Biol. *14*, 249–250.

Shalaby, F., Rossant, J., Yamaguchi, T.P., Gertsenstein, M., Wu, X.F., Breitman, M.L., and Schuh, A.C. (1995). Failure of blood-island formation and vasculogenesis in Flk-1-deficient mice. Nature *376*, 62–66.

Shibuya, M., Yamaguchi, S., Yamane, A., Ikeda, T., Tojo, A., Matsushime, H., and Sato, M. (1990). Nucleotide sequence and expression of a novel human receptor-type tyrosine kinase gene (flt) closely related to the fms family. Oncogene *5*, 519–524.

Spratlin, J.L., Cohen, R.B., Eadens, M., Gore, L., Camidge, D.R., Diab, S., Leong, S., O'Bryant, C., Chow, L.Q., Serkova, N.J., et al. (2010). Phase I pharmacologic and biologic study of ramucirumab (IMC-1121B), a fully human immunoglobulin G1 monoclonal antibody targeting the vascular endothelial growth factor receptor-2. J. Clin. Oncol. *28*, 780–787.

Tammela, T., and Alitalo, K. (2010). Lymphangiogenesis: molecular mechanisms and future promise. Cell *140*, 460–476.

Terman, B.I., Carrion, M.E., Kovacs, E., Rasmussen, B.A., Eddy, R.L., and Shows, T.B. (1991). Identification of a new endothelial cell growth factor receptor tyrosine kinase. Oncogene *6*, 1677–1683.

Terman, B.I., Dougher-Vermazen, M., Carrion, M.E., Dimitrov, D., Armellino, D.C., Gospodarowicz, D., and Böhlen, P. (1992). Identification of the KDR tyrosine kinase as a receptor for vascular endothelial cell growth factor. Biochem. Biophys. Res. Commun. *187*, 1579–1586.

Uysal, H., Sehnert, B., Nandakumar, K.S., Böiers, U., Burkhardt, H., Holmdahl, R., and Thunnissen, M.M. (2008). The crystal structure of the pathogenic collagen type II-specific mouse monoclonal antibody CIIC1 Fab: structure to function analysis. Mol. Immunol. *45*, 2196–2204.

Wiesmann, C., Fuh, G., Christinger, H.W., Eigenbrot, C., Wells, J.A., and de Vos, A.M. (1997). Crystal structure at 1.7 Å resolution of VEGF in complex with domain 2 of the Flt-1 receptor. Cell *91*, 695–704.

Wilhelm, S.M., Carter, C., Tang, L., Wilkie, D., McNabola, A., Rong, H., Chen, C., Zhang, X., Vincent, P., McHugh, M., et al. (2004). BAY 43-9006 exhibits broad spectrum oral antitumor activity and targets the RAF/MEK/ERK pathway and receptor tyrosine kinases involved in tumor progression and angiogenesis. Cancer Res. *64*, 7099–7109.

Wilhelm, S.M., Adnane, L., Newell, P., Villanueva, A., Llovet, J.M., and Lynch, M. (2008). Preclinical overview of sorafenib, a multikinase inhibitor that targets both Raf and VEGF and PDGF receptor tyrosine kinase signaling. Mol. Cancer Ther. *7*, 3129–3140.

Witte, L., Hicklin, D.J., Zhu, Z., Pytowski, B., Kotanides, H., Rockwell, P., and Böhlen, P. (1998). Monoclonal antibodies targeting the VEGF receptor-2 (Flk1/KDR) as an anti-angiogenic therapeutic strategy. Cancer Metastasis Rev. *17*, 155–161.

Yuzawa, S., Opatowsky, Y., Zhang, Z., Mandiyan, V., Lax, I., and Schlessinger, J. (2007). Structural basis for activation of the receptor tyrosine kinase KIT by stem cell factor. Cell *130*, 323–334.

